Continuous gas temperature measurement of cold plasma jets containing microdroplets, using a focussed spot IR sensor

Hendawy, N., McQuaid, H., Mariotti, D., & Maguire, P. (2020). Continuous gas temperature measurement of cold plasma jets containing microdroplets, using a focussed spot IR sensor. *Plasma Sources Science and Technology*, *29*(8), [085010]. https://doi.org/10.1088/1361-6595/aba2aa

Link to publication record in Ulster University Research Portal

Published in:
Plasma Sources Science and Technology

Publication Status:
Published online: 13/08/2020

DOI:
10.1088/1361-6595/aba2aa

Document Version
Author Accepted version

General rights
Copyright for the publications made accessible via Ulster University's Research Portal is retained by the author(s) and / or other copyright owners and it is a condition of accessing these publications that users recognise and abide by the legal requirements associated with these rights.

Take down policy
The Research Portal is Ulster University's institutional repository that provides access to Ulster's research outputs. Every effort has been made to ensure that content in the Research Portal does not infringe any person's rights, or applicable UK laws. If you discover content in the Research Portal that you believe breaches copyright or violates any law, please contact pure-support@ulster.ac.uk.

Download date: 04/05/2023

Plasma Sources Science and Technology

ACCEPTED MANUSCRIPT

Continuous gas temperature measurement of cold plasma jets containing microdroplets, using a focussed spot IR sensor

To cite this article before publication: Nourhan Hendawy *et al* 2020 *Plasma Sources Sci. Technol.* in press https://doi.org/10.1088/1361-6595/aba2aa

Manuscript version: Accepted Manuscript

Accepted Manuscript is "the version of the article accepted for publication including all changes made as a result of the peer review process, and which may also include the addition to the article by IOP Publishing of a header, an article ID, a cover sheet and/or an 'Accepted Manuscript' watermark, but excluding any other editing, typesetting or other changes made by IOP Publishing and/or its licensors"

This Accepted Manuscript is **© 2020 IOP Publishing Ltd**.

During the embargo period (the 12 month period from the publication of the Version of Record of this article), the Accepted Manuscript is fully protected by copyright and cannot be reused or reposted elsewhere.
As the Version of Record of this article is going to be / has been published on a subscription basis, this Accepted Manuscript is available for reuse under a CC BY-NC-ND 3.0 licence after the 12 month embargo period.

After the embargo period, everyone is permitted to use copy and redistribute this article for non-commercial purposes only, provided that they adhere to all the terms of the licence https://creativecommons.org/licences/by-nc-nd/3.0

Although reasonable endeavours have been taken to obtain all necessary permissions from third parties to include their copyrighted content within this article, their full citation and copyright line may not be present in this Accepted Manuscript version. Before using any content from this article, please refer to the Version of Record on IOPscience once published for full citation and copyright details, as permissions will likely be required. All third party content is fully copyright protected, unless specifically stated otherwise in the figure caption in the Version of Record.

View the article online for updates and enhancements.

This content was downloaded from IP address 2.221.92.115 on 21/07/2020 at 10:03

Continuous gas temperature measurement of cold plasma jets containing microdroplets, using a focussed spot IR sensor

N. Hendawy[1], H McQuaid[1], D. Mariotti[1], P Maguire[1]

[1]NIBEC, University of Ulster, Belfast, BT37 0QB, Northern Ireland

Abstract

Controlling gas temperature via continuous monitoring is essential in various plasma applications especially for biomedical treatments and nanomaterial synthesis but traditional techniques have limitations due to low accuracy, high cost or experimental complexity. We demonstrate continuous high-accuracy gas temperature measurements of low-temperature atmospheric pressure plasma jets using a small focal spot infrared sensor directed at the outer quartz wall of the plasma. The impact of heat transfer across the capillary tube was determined using calibration measurements of the inner wall temperature. Measured gas temperatures varied from 25 ºC – 50 ºC, increasing with absorbed power and decreased gas flow. The introduction into the plasma of a stream (~10^5 s^{-1}) of microdroplets, in the size range 12 µm – 15 µm, led to a reduction in gas temperature of up to 10 ºC, for the same absorbed power. This is an important parameter in determining droplet evaporation and its impact on plasma chemistry.

Introduction

Continuous and reliable measurement of gas temperature in atmospheric pressure plasmas (APP) is critical for future applications in plasma medicine, food and agriculture as well as nanomaterials synthesis. APP systems cover a wide variety of configurations, geometries and temperature ranges. In non-thermal equilibrium APPs there is generally a desire to maintain temperatures as low as possible. However, there is also an understanding that gas temperature can be sensitive to many factors that are rarely well-characterised or controlled, especially with the inclusion of molecular gases and water as environmental feedback factors. Gas temperature increase in APPs is due to the high electron and particle collisionality of these systems.[1] Most chemical and combustion reactions are strongly dependent on gas temperature,[2] as are surface reactions and neutral radical distributions and their kinetics.[3,4] Additionally in many biomedical and material applications a controlled heat load is required for the treatment of heat sensitive surfaces e.g. wound tissue and polymers.[5] Issues such as feedback process control, process stability/repeatability, regulatory, or end-user approval, require a capability for inline monitoring of temperature and rapid response to fluctuations or thermal runaway.

The various techniques to measure gas temperature include optical emission spectroscopy (OES),[1,6–15] infrared thermometry,[1,16–18] millimetre wave interferometry,[19] Schlieren,[1,5] Rayleigh scattering,[20,21] thermocouple,[1,11,22,23] and fibre optic based thermometry[24,25]. These have been applied to a varying degree in different plasma systems including plasma torch [15,26,27], dielectric barrier discharge,[1,7,14,18,19] plasma jet, [5,8,9,16,20,24,27,28] gliding arc discharge,[2,17,25] and glow discharge.[21] While some methods offer high accuracy, they are not suitable for continuous measurement due to size and cost and have generally been used to provide a calibrated reference for other techniques, particularly OES, which is a routine and non-invasive technique. OES obtains a gas temperature estimate by fitting the experimental spectra to theoretical spectra of chosen molecular species, for example N_2, NO, OH or CN.[20,27] However the population of the rotational energy levels, derived from the observed emission cannot automatically be assumed to be in equilibrium with the translational states i.e. gas temperature.[2,28] Iseni et al.[29] compared the analysis of broadening (line, resonance and Van der Waals) of specific isolated lines with the analysis of the rotational distribution of diatomic molecules as methods to determine neutral gas temperatures. They provide estimates of uncertainties of 3% - 6% and 4% respectively. Since high resolution spectrometer instrumentation is not viable for continuous sensing, the inability to resolve the rotational structures leads to a fitting process which can be complex, slow, difficult to automate,

Accepted Manuscript

and with accuracy levels strongly dependent on apparatus parameters.[2,27] Temperature resolution is of the order ≥ 50 K in cold plasmas unless high resolution spectra are available.

Other potential inline measurement techniques such as thermocouple (TC), fibre optic (FO) thermal indicators and traditional infrared-emission (IR) are also problematic.[30] Permanently locating the TC or FO into the gas stream is often inhibited by geometric restrictions, flow disruption, contamination and electrical coupling concerns. Traditional IR measurements provide an average wall temperature value over the field of view (FoV) and at typical sensor stand-off distances, the FoV is unsuitable for many plasma systems because of size or temperature non-uniformity. Thermal imaging using cooled high resolution IR cameras can improve the spatial resolution but this technique is reserved for stand-alone experiments, often at high temperatures.[31–35]

Previously we have used OES spectra of OH lines to determine the impact of APP heating on nanoparticle synthesis with an estimated fit error of ±50 K, for temperatures around 600 K in dry Ar.[36] However, with added water, the use of the OH lines leads to heightened error margins due to electronic quenching of OH (A-X) emission by H_2O molecules.[37] This effect becomes noticeable at 100 – 300 ppm H_2O and above.[38] Microdroplet transport through plasma jets can generate beneficial enhancement and transport of radical species (e.g. $OH^{\bullet}$, H_2O_2), important electron reduction reactions and rapid nanomaterials synthesis.[39,40] The chemical kinetics are thought to depend on droplet evaporation which in turn is sensitive to gas temperature. However the OES derived temperature estimates, obtained using OH lines, exhibit significant differences compared to using the N_2 lines, once droplets are introduced into the plasma.[6] Here we investigate the use of a small form factor IR sensor for continuous monitoring of gas temperature of a RF plasma jet contained in a narrow quartz capillary tube. The plasma region is defined by two outer ring electrodes which are separated by a distance ≥ 2 mm. The sensor FoV diameter is 0.6 mm at a stand-off distance of 10 mm. It is expected that the inner wall temperature of the capillary in contact with the plasma will rapidly reach equilibrium with the plasma gas temperature and represent a close approximation. In order to determine the temperature gradient across the quartz, i.e. between inner and outer walls, we first measure the temperature of the inner wall in contact with the plasma with the sensor placed at the capillary exit and directed along the capillary axis. Precisely locating the sensor FoV within the plasma region is achieved with reference to a known geometrical setup, by scanning the sensor in XYZ directions and over a range of angles. After obtaining calibration measurements of outer wall against inner wall temperature for varying power, flow and He/Ar gas mixture, we then determine gas temperature in the presence of microdroplets from the outer wall temperature.

Methods

Figure 1 shows a schematic and a photo of the experimental apparatus. The plasma is generated inside a capillary quartz tube 2.00 mm inner diameter (0.2 mm thickness). Radio frequency (RF) power at 13.56 MHz is connected to two concentric copper ring electrodes with a 2 mm separation, with the quartz tube extending 1 mm below the lower electrode. He, Ar and Ar/He gas flows from 0.5 to 3.0 slm without droplets were controlled by MKS G-Series mass flow controller. The net RF power, as determined using an Octiv Suite 2.0 VI Probe, is varied from 0.05 W to 0.6 W. For microdroplet studies, microdroplets with average diameters in the range 12 μm – 15 μm were obtained from a Burgener Mira Mist X-175 nebuliser and were injected into a helium gas flow (Q_1) of 0.7 slm upstream of the plasma. The nebuliser was driven by a separate He gas flow (Q_2) and the total plasma gas flow was $Q = Q_1 + Q_2$. The liquid (H_2O) was supplied from a syringe pump at 4 μl/min and an estimated 5×10^4 droplets per second were delivered into the plasma.[6,39] Infrared temperature measurements were obtained using a Micro-Epsilon Thermometer CT precise infrared sensor (CT-CF22-C1 Miniature-Pyrometer) with spectral range 8 - 14 μm and integrated CF lens providing a focal spot diameter of 0.6 mm at a stand-off distance of 10 mm.[41]

Accepted Manuscript

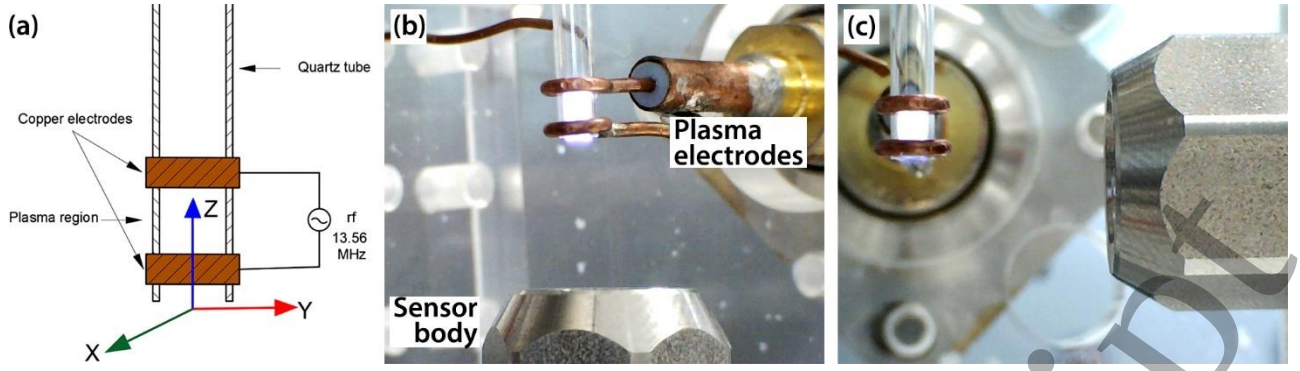

Figure 1. *(*a) Schematic of the plasma setup with axis labels, *(*b) vertical orientation for inner wall temperature measurement and (c) horizontal orientation for outer wall measurement.

In normal operation, the sensor face is positioned at a stand-off distance from the outer wall of the quartz tube to collect emission from between the copper electrodes, figure 1(c). In order to calibrate the temperature gradient across the thin quartz wall, calibration measurements of the inner wall temperature between the electrodes are obtained with the setup shown in figure 1(b), with the sensor pointing upwards along the capillary axis. The variation in sensor FoV with stand-off distance is given in figure 2(a) and the sensor position relative to the capillary exit, in the configuration of figure 1(b), is shown in the CAD drawing of figure 2(b), with the optic field profile overlaid (red). The 7 mm wide sensor face is inclined at angle θ with its centreline situated X mm and Y mm from the capillary axis and Z mm from the capillary exit. To obtain an optic field intersection with the inner wall, of diameter D, within the region bounded by the two electrodes, the sensor XYZ position and angle θ is varied in increments of 0.25 mm and 0.5 degrees, respectively. The clearance, c, between the upper edge of the optic field and the bottom of the quartz tube determines the limit of sensor vertical movement. Firstly, the precise centreline (axis) of the tube is determined by scanning the sensor in x- and y-directions with a nominal 0^o inclination. The resultant temperature profile, figure 3(a) shows two peaks indicating the wall positions and the centreline is assumed to be at the lowest temperature between the walls. The sensor is then positioned at this centreline axis and the temperature is obtained while the inclination is varied using a precision rotation platform (5 arcmin resolution), figure 3(b). The reference 0^o inclination is taken as the angle at which the minimum temperature occurs.

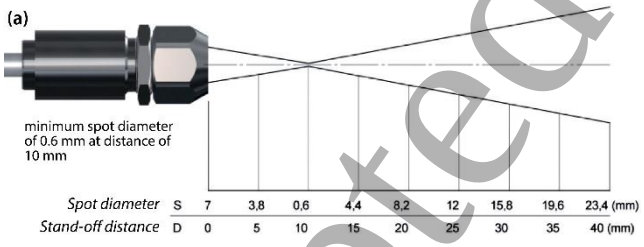

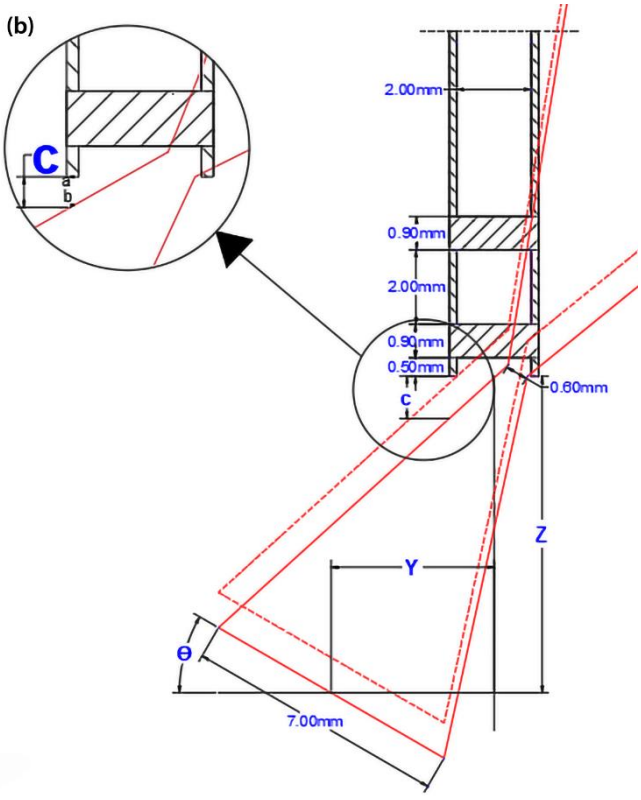

Accepted Manuscript

Figure 2. (a) IR sensor optic field profile showing spot diameter versus stand-off distance and (b) CAD drawing of the geometric setup of the plasma capillary and IR probe, in vertical configuration for inner wall measurement. Overlay shows the positions of the optic field profile outlines, initially (red, dashed) and after translation in the Z-axis (red, solid), where the initial clearance between upper edge of the optic field and quartz wall is 0 mm and the final clearance is c mm.

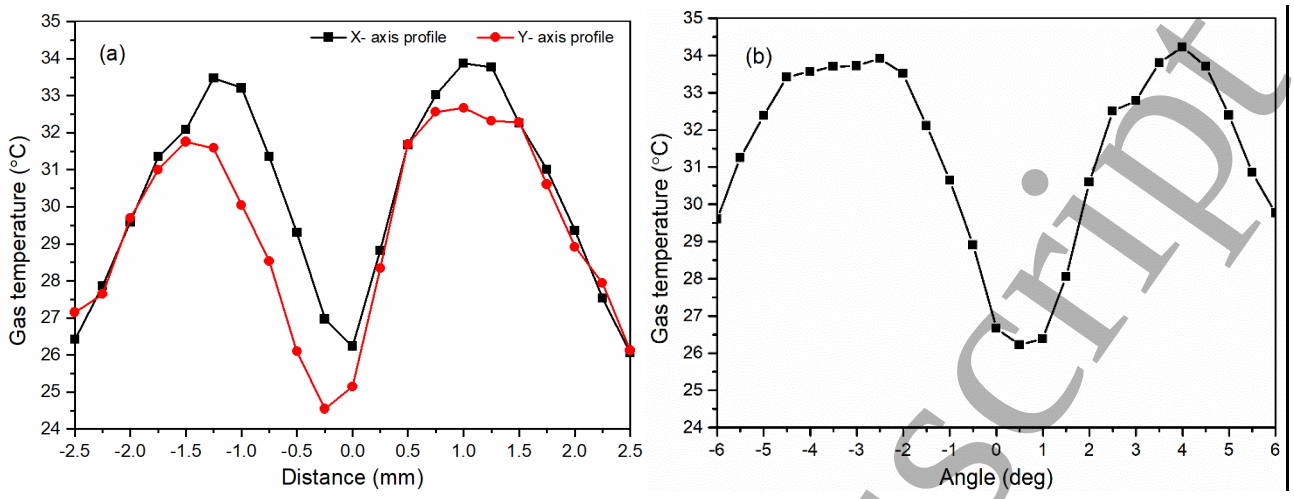

Figure 3. Determining the alignment of sensor with respect to the quartz tube axis from temperature profiles across the tube by (a) varying X and Y distances and (b) angle of inclination

To locate its normal position reading the outer wall temperature at the centre of the plasma, the sensor is set at a stand-off distance of 10 mm, with an FoV diameter at the outer quartz wall of 0.6 mm, figure 1(c). The sensor is scanned in the horizontal direction (X), to determine the tube limits and central axis, and in the vertical direction to locate the two electrodes and obtain plasma temperatures in the interval. The temperature peaks in the z-axis profile of figure 4 represent the Cu electrodes. The actual value of temperature is unknown since the emissivity of Cu varies considerably (0.1 to 0.9) based on surface condition. Assuming a Cu emissivity range of 0.5 to 0.8 for unpolished/rolled metal, gives a maximum upper electrode temperature in the range 50 °C – 80 °C. The distance between temperature peaks in the vertical (Z) profile, figure 4, is ~3 mm, equivalent to the 2 mm gap between electrodes and accounting for electrode thickness and FoV diameter. The constant temperature valley extends ~1.5 mm and this provides the average plasma temperature.

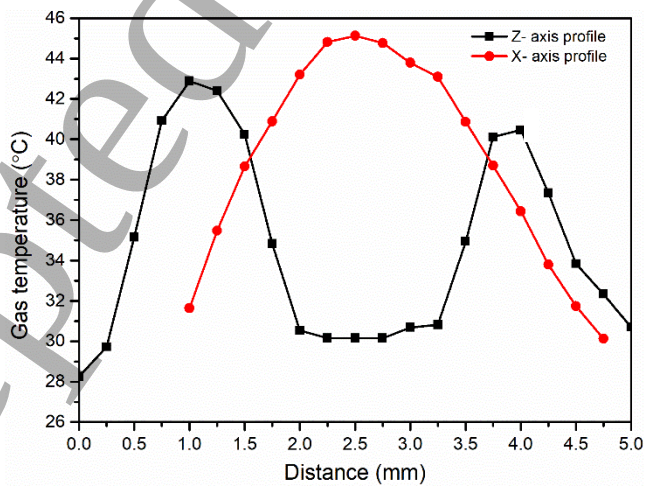

Figure 4. Vertical and horizontal temperature profile of the outer surface of the capillary with the IR probe in the horizontal position. The peaks in the z-axis profile indicate the Cu electrode temperature. An emissivity value of 0.93 (quartz) was used and temperature values are valid only for the quartz region. Assuming a Cu emissivity range of 0.5 to 0.8 for unpolished/rolled metal, gives a maximum upper electrode temperature in the range 50 °C – 80 °C.

The IR sensor readings are available every 1 ms. Transient thermal response characteristics are shown in figure 5 for both inner and outer wall measurements. Plasma ignition and extinction points are

Accepted Manuscript

obtained from a photodiode response to plasma brightness. The rise time to final average value is ~3 s for both. For all temperature measurements, a constant quartz emissivity value of 0.93 was used.

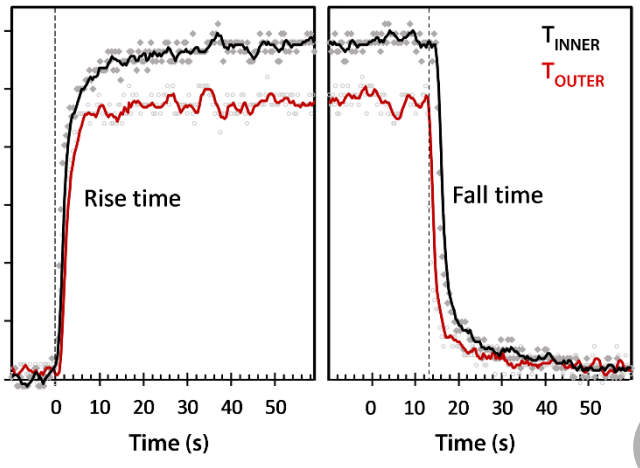

Figure 5. Temperature rise and fall times for inner wall (black) and outer wall (red). Dashed lines indicate the plasma ignition and extinction times obtained from photodiode response.

Results

Plasma only

After locating the sensor centreline point of the tube, the aim was to adjust the XYZ and θ positions to achieve an intersection of the optical field with the inner wall that lies between the two electrodes. The sensor starting positions are chosen to ensure the optical edge at the minimum spot size is located as close as possible to the end of the tube inner wall. Three example starting positions are illustrated in figure 6 and Y(0), Z(0) and θ(0) initial values along with the resultant focal spot diameter, D, is given in Table 1. The dashed optic field profile indicates the limit of Z-travel while maintaining c > 0. The inner wall temperature profile, figure 7, was obtained for each starting setup in figure 6, by varying the clearance, c, from zero up to the maximum possible, given in Table 1. Profile A is dominated by the temperature at the lower electrode region and is constant with c. The profile C diameter at the wall is > 4 mm and hence is greater than the plasma area. The temperature increases as the spot moves down since less of the cooler wall above the plasma region is included in the temperature measurement. In profile B, the spot size and location represent the closest match to the plasma region. The temperature decreases as the spot moves away from the powered electrode. The final position is taken therefore from the maximum temperature point of profile B and is given by Y = 4.91 mm, Z = 8.15 mm, θ = 33.75, c ~ 0 mm, with a spot diameter of 2.94 mm.

	Y(0) mm	**Z(0) mm**	**Θ(0)**	**c(final) mm**	**D mm**
Profile A	6.10	6.78	42.69°	0.42	1.75
Profile B	4.91	8.15	33.75°	0.78	2.94
Profile C	4.37	8.51	30.05°	0.94	4.05

Table 1. Values for initial IR sensor positions and inclinations according to CAD drawings in Figure 6. X and Y are the distances (mm) from the capillary centreline, Z is the distance from the sensor to the capillary, c is the clearance before the optic field hits the wall, Θ is the angle of inclination with x-axis and D is the diameter of optical spot in mm.

Accepted Manuscript

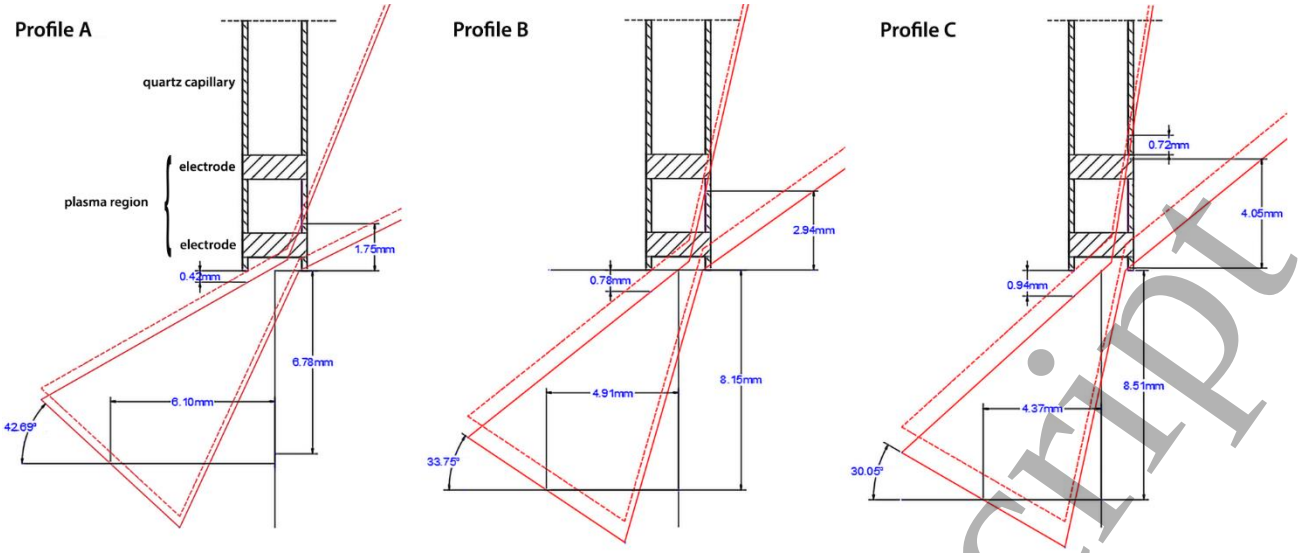

Figure 6. CAD drawings of initial IR sensor positions and inclinations showing the intersection of optical field with inner wall. The optical field profile (solid red) is obtained from manufacturers specifications (see Fig 2(a)), the dashed lines indicate maximum Z-axis travel for c > 0.

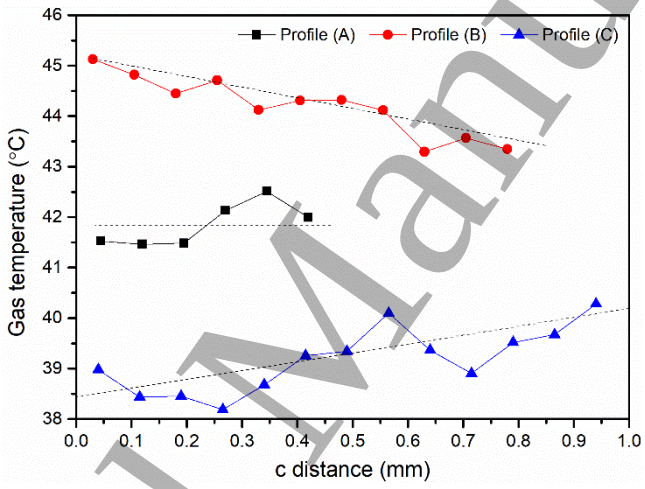

Figure 7. Temperature profile of the inner wall of the capillary tube versus clearance, c, between bottom of quartz tube and the upper edge of the optic field profile (see Fig 2(b)). Note in Figure 6, the minimum clearance is shown by the dashed profile and maximum by the solid.

In a He plasma, the average temperature variation with power, figure 8(a), follows an almost linear relationship with minimal difference between inner and outer wall temperatures while for argon, a sub-linear relation is observed and the outer wall temperature is 2 ^{o}C – 4 ^{o}C higher than the inner. The temperature differences between inner and outer wall are of similar magnitude to error margin of individual readings. Nevertheless, there is evidence that the plasma electrode temperature increases when the plasma is operated with argon. This may cause some external heating of the quartz capillary. With increasing flow, the gas temperature decreases for both gases, figure 9. The introduction of Ar into He changes the plasma impedance and at the lowest flow rate, the gas temperature falls to a minimum when the Ar:He fraction reaches 40:60, figure 10. A plot of net power absorbed against mixture ratio shows the temperature fall is due to a reduction in absorbed power with mixture variation.

We also obtained thermocouple (TC) measurements close to the gas outlet. Using an unshielded Type K thermocouple resulted in large inaccuracies due to RF interference. To overcome this an earthed shield was incorporated around the TC tip, which was set ~20 mm from the outlet of a similar plasma configuration which had a greater clearance to accommodate the bulky TC. Measurements required up to 300 s to reach equilibrium and the final measured temperature variation with power at 1 slm flow was from 34 ^{o}C to 55 ^{o}C. Finally, a number of different insulating probes were placed at the gas outlet

Accepted Manuscript

and temperature stabilised in the gas flow. One probe consisted of a polymer tube of diameter ~1 mm covered with black tape while the other was a thin 0.5 mm black insulated wire. The IR sensor, in vertical mode, figure 1(b), was then focussed on these probes and a temperature reading obtained. An emissivity value of 1 was assumed for both. In He (0.58W, 0.5 slm) the measured temperature was 38 °C and 49 °C for the tube and wire respectively, while the inner wall temperature at these conditions was 44 °C to 46 °C. In Ar (0.58W, 0.5 slm) the measured temperature was 36 °C and 39 °C for the tube and wire respectively, while the inner wall temperature at these conditions was 43 °C to 45 °C.

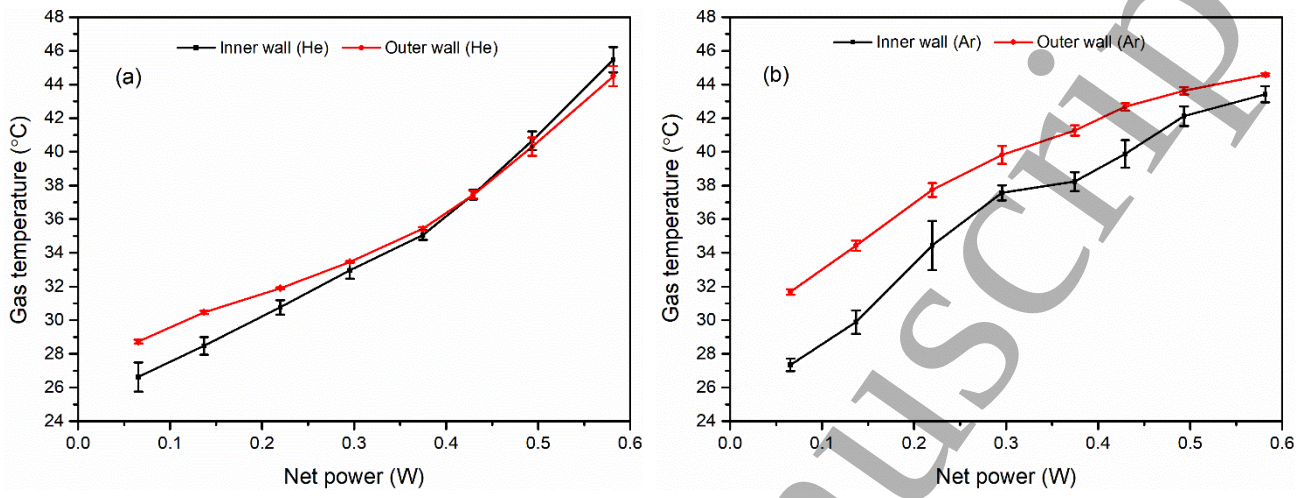

Figure 8. Inner and outer wall temperature of the capillary tube against RF net power at a fixed flow rate of 1.0 slm for (a) He and (b) Ar plasmas. Error bars represent the standard error (n = 3)

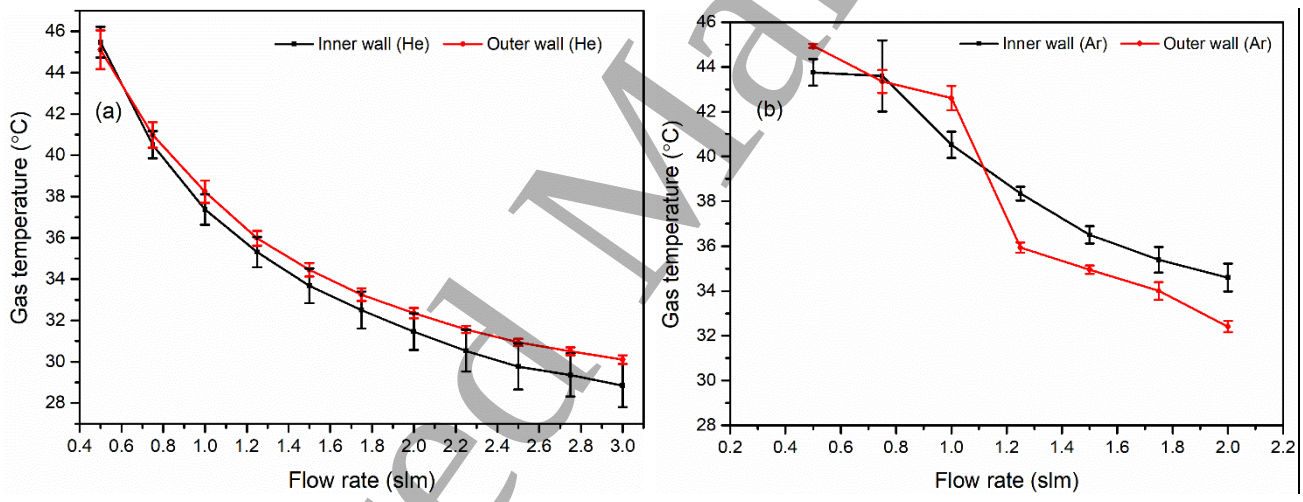

Figure 9. Inner and outer wall temperature of the capillary tube against flow rate at a fixed RF net power of 0.3W for (a) He and (b) Ar plasmas. Error bars represent the standard error (n = 3)

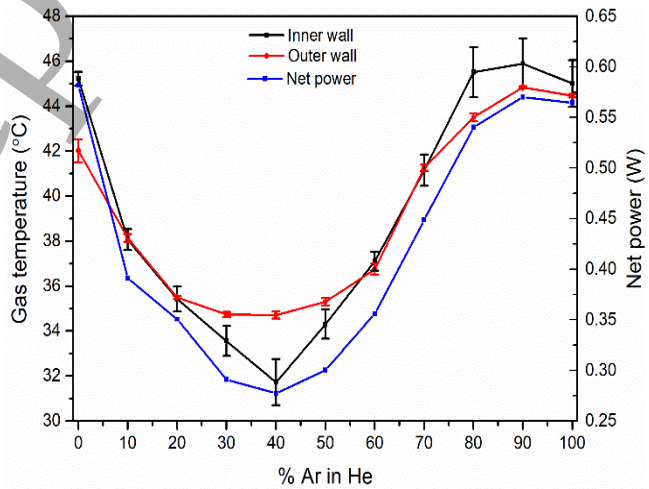

Accepted Manuscript

Figure 10. Inner wall temperature versus Ar:He mixture at total flow rate of 1.5 slm and maximum net power of 0.58 W. Also shown is the variation in absorbed power with Ar:He ratio. Error bars represent the standard error (n = 3)

Plasma with microdroplets

Inclusion of microdroplets into the plasmas causes a reduction of the gas temperature. For a total He gas flow of 1.5 slm, the absolute temperature decreased by ≥ 6 °C at the lowest power and by 12 °C at the highest power, figure 11. The temperature sensitivity to power variation was also reduced. The reduction in temperature with the addition of microdroplets was most noticeable at the lower flow rates, figure 12. At the highest flow (3 slm) the temperature difference was ~1 °C.

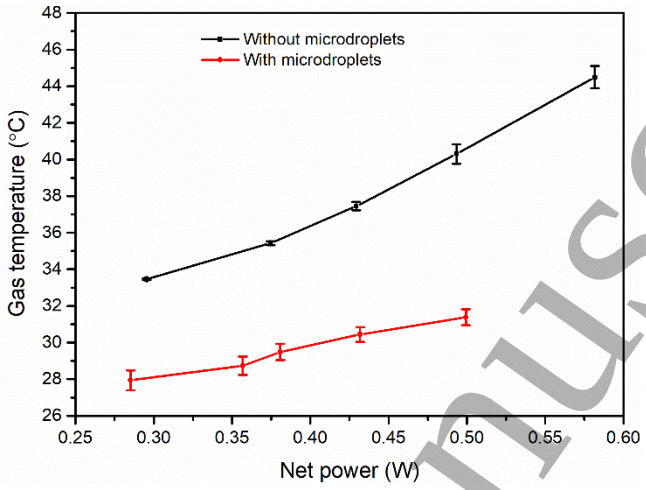

Figure 11. Gas temperature against RF net power in He without and with microdroplets at flow rates of 1.5 slm. Error bars represent the standard error (n = 3)

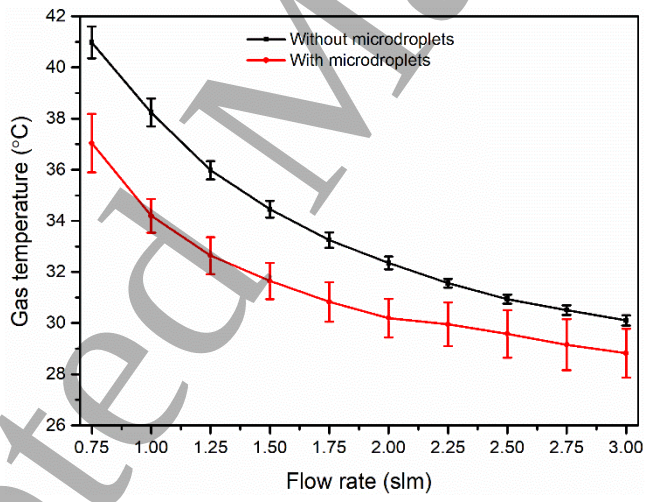

Figure 12. Gas temperature versus total He gas flow rate with and without microdroplets, for a fixed RF power of 0.3W. Error bars represent the standard error (n = 3)

Discussion

The use of plasma-exposed microdroplets has important potential for delivering plasma-activated liquids and on-demand nanoparticles downstream over rapid timescales. Their chemistry, lifetime and transport however will be sensitive to the gas temperature in the plasma. It is well-known that the addition of small quantities of electronegative gases, e.g. O_2 or H_2O, can increase the gas temperature in noble gas plasmas[2,42] and hence the possibility exists for accelerated gas heating as the droplet evaporation proceeds. However, under current conditions, the reduction in gas temperature with microdroplet addition indicates that other factors, including evaporative cooling, may be involved. The significance of such cooling depends on droplet number and evaporation rate.

Accepted Manuscript

We have previously estimated average droplet evaporation rates by comparing lognormal droplet size and velocity distributions with and without plasma exposure and fitting to a D^2 – time profile.[6,39] For the conditions in this study, the evaporation rate was ~5 x 10^{-8} m^2 s^{-1}. The maximum droplet rate, obtained from the liquid flow rate and the droplet size distribution, is 5 x 10^4 s^{-1} and the total energy flux (power) required, from the plasma, for this level of evaporation is 18 mW. For the case where droplet and gas travel at same velocity, we used a simplified version of the Abramzon and Sirignano model for droplet vaporisation which indicated that gas heating supplies a maximum energy flux of 3 mW, i.e. over 80% of the evaporation is due to droplet bombardment by charged species.[43] Heinisch et al. observed experimental evaporation rates in flowing dry N_2, without plasma, approximately one order of magnitude lower than found here, supporting the conclusion that evaporation is dominated by charged particle heating of the droplet.[44]

We observed a reduction in gas temperature when droplets are introduced while the power absorbed remains constant. From heat capacity considerations, the maximum difference in temperature (10 °C at 1.5 SLM and 0.3 W) is equivalent to a power difference of 200 mW. At the highest flow, the small reduction in temperature is equivalent to ~40 mW. Therefore across all conditions, the contribution of evaporative cooling (18 mW) is insufficient to account for the full temperature reduction. The introduction of electronegative gases is known to affect power absorption efficiency as the plasma couples less effectively to negative ions. In a separate study, we have observed this effect as H_2O content in the plasma reaches ~3000 ppm. However, with a maximum droplet flow rate of 5 x 10^4 s^{-1}, the evaporation contributes a maximum of 23 ppm to the average H_2O content in the plasma and hence the impact of enhanced humidity is negligible. Although the evaporated water is more likely to diffuse slowly away from the droplet, ~ 100 μm over the plasma flight time, rather than disperse uniformly throughout, the vast majority of the plasma volume remains in its original dry and electropositive state.

Plasma ion density variation also impacts on gas temperature through ion – neutral collisions.[20,42,44] Figure 8(a) shows an almost linear relationship between gas temperature and power, for He, and we expect plasma density to scale linearly with absorbed power. In figure 8(b), Ar, the relationship is sub-linear. On introducing droplets, any reduction in plasma density while constant power is maintained implies that the loss terms in the power balance equation increase; these include collisional energy lost per electron-ion pair created and the mean kinetic energy lost per electron or ion lost, which depends on T_e. Therefore droplet introduction may lead to a reduction in plasma density and increase in electron temperature, while the absorbed power remains approximately constant.

Successful implementation of droplet in plasma (DiP) technology for application in areas such as plasma medicine, agriculture and microreaction chemistry requires knowledge and control of gas temperature and evaporation kinetics. Future developments include increasing droplet flow rate while reducing diameter, gas velocity and extending the plasma flight time. Under current conditions only the smaller droplets (< 4 μm) evaporated totally, resulting in a loss of ~5% of the total droplet number and ~0.05% of the total liquid flow volume. For a ten-fold increase in droplet rate and a reduction to an average diameter of 5 μm, while maintaining constant gas flow, the added water content increases to 2000 ppm while the evaporative cooling power also increases to ~700 mW. This provides an indication of the future scope for parameter optimisation.

Conclusions

Continuous gas temperature measurement in plasmas is important for many applications, particularly for verifiable monitoring and control of plasmas for medical treatment. We have shown the accurate measurement of gas temperature using a small-spot IR temperature probe focussed on the outer quartz wall. Calibration was obtained via careful measurement of the temperature of the inner wall in direct contact with the plasma, to account for heat loss across the thin quartz tube. For He plasmas, the temperature difference between inner and outer walls was not detectable, within the error margin. For

Accepted Manuscript

argon, the outer wall was a few degrees hotter. This may be due to additional heating by the external electrodes, since the Ar required greater applied power for the same net power. While the emissivity of quartz is reasonably constant at 0.93, Cu emissivity can vary widely depending on surface condition of the metal. We estimate the electrode temperature between 50 ^{o}C and 80 ^{o}C. Electrode heating of the quartz outer surface may therefore lead to an overestimation of gas temperature. Plasma gas temperature was observed to increase, as expected, with increasing power and reduced gas flow. The maximum temperature over the full operating range was < 50 ^{o}C and little difference was observed between pure He and Ar plasmas. For Ar/He mixtures, the fall in temperature on adding Ar is clearly due to the reduction in absorbed power caused by a change in the electrical characteristics of the plasma. The non-invasive low-cost IR probe demonstrated sub-second resolution and performs much better than bulky shielded thermocouple probes that obstruct the gas flow and have a response time of many minutes. Compared to expensive thermal image cameras that can resolve small plasma dimensions, the small-spot IR sensor can be kept in-situ and its output directly used for feedback control. The sensor also provides useful temperature information for more complex plasma configurations. We observe a cooling of the plasma on introduction of a microdroplet stream. Previous estimates of such temperatures using OES fitting had a wide error margin (~50 ^{o}C) and suggested an average of >75 ^{o}C. This is an important parameter in modelling the droplet evaporation rate and the resultant enhancement of overall humidity. The observed fall can be attributed to evaporative cooling and since an increase in humidity generally leads to increased gas heating, these results indicate that the average humidity remains approximately constant and confirms previous droplet measurements which show limited size reduction due to evaporation during transit through the plasma.[6]

References

1. Zhou S, Su L, Shi T, et al. Experimental study on the diffusive flame stabilization mechanism of plasma injector driven by AC dielectric barrier discharge. *J Phys D Appl Phys*. 2019;52(26). doi:10.1088/1361-6463/ab15cd

2. Bruggeman PJ, Sadeghi N, Schram DC, Linss V. Gas temperature determination from rotational lines in non-equilibrium plasmas: A review. *Plasma Sources Sci Technol*. 2014;23(2). doi:10.1088/0963-0252/23/2/023001

3. Aramaki M, Okumura Y, Goto M, Muto S, Morita S, Sasaki K. Measurements of gas temperature in high-density helicon-wave H2 plasmas by diode laser absorption spectroscopy. *Japanese J Appl Physics, Part 1 Regul Pap Short Notes Rev Pap*. 2005;44(9 A):6759-6763. doi:10.1143/JJAP.44.6759

4. Fridman AA, Boufendi L, Hbid T, Potapkin B V., Bouchoule A. Dusty plasma formation: Physics and critical phenomena. Theoretical approach. *J Appl Phys*. 1996;79(3):1303-1314. doi:10.1063/1.361026

5. Schmidt-Bleker A, Reuter S, Weltmann KD. Quantitative schlieren diagnostics for the determination of ambient species density, gas temperature and calorimetric power of cold atmospheric plasma jets. *J Phys D Appl Phys*. 2015;48(17):175202. doi:10.1088/0022-3727/48/17/175202

6. Maguire PD, Mahony CMO, Kelsey CP, et al. Controlled microdroplet transport in an atmospheric pressure microplasma. *Appl Phys Lett*. 2015;106(22). doi:10.1063/1.4922034

7. Yoon SY, Yi C, Eom S, et al. Effects of gas temperature in the plasma layer on RONS generation in array-type dielectric barrier discharge at atmospheric pressure. *Phys Plasmas*. 2017;24(12). doi:10.1063/1.5003205

8. Bazavan M, Teodorescu M, Dinescu G. Confirmation of OH as good thermometric species for gas temperature determination in an atmospheric pressure argon plasma jet. *Plasma Sources Sci*

Accepted Manuscript

Technol. 2017;26(7). doi:10.1088/1361-6595/aa723c

9. Walsh JL, Kong MG. Room-temperature atmospheric argon plasma jet sustained with submicrosecond high-voltage pulses. *Appl Phys Lett*. 2007;91(22):2005-2008. doi:10.1063/1.2817965

10. Mariotti D, Shimizu Y, Sasaki T, Koshizaki N. Gas temperature and electron temperature measurements by emission spectroscopy for an atmospheric microplasma. *J Appl Phys*. 2007;101(1):1-8. doi:10.1063/1.2409318

11. Gulec A, Bozduman F, Hala AM. Atmospheric Pressure 2.45-GHz Microwave Helium Plasma. *IEEE Trans Plasma Sci*. 2015;43(3):786-790. doi:10.1109/TPS.2015.2403280

12. Tuszewski M. Ion and gas temperatures of 0.46 MHz inductive plasma discharges. *J Appl Phys*. 2006;100(5):0-5. doi:10.1063/1.2337167

13. Jayapalan KK, Chin OH. Measurement of neutral gas temperature in a 13.56 MHz inductively coupled plasma. *AIP Conf Proc*. 2015;1657. doi:10.1063/1.4915242

14. Hu Y, Yang J, Feng C, et al. A Convenient Method to Realize Large-Area APGD for Wool Surface Modification. *IEEE Trans Plasma Sci*. 2019;47(5):2629-2636. doi:10.1109/TPS.2019.2907099

15. Li SZ, Li ZY, Wu Y, Zhang J. Spectroscopic diagnosis of gas temperature in blown-out plasma of atmospheric-pressure microwave oxygen plasma torch. *Phys Plasmas*. 2018;25(1). doi:10.1063/1.5009591

16. Li X, Yuan N, Jia P. Investigation of a plasma jet generated by high voltage discharge at atmospheric pressure. *Adv Mater Res*. 2012;383-390:5907-5911. doi:10.4028/www.scientific.net/AMR.383-390.5907

17. Sláma J. Plasma flow and temperature in a gliding reactor with different electrode configurations. *Acta Polytech*. 2012;52(1):61-64. doi:10.14311/1516

18. Brehmer F, Welzel S, Van De Sanden MCM, Engeln R. CO and byproduct formation during CO2 reduction in dielectric barrier discharges. *J Appl Phys*. 2014;116(12). doi:10.1063/1.4896132

19. Lu XP, Laroussi M. Electron density and temperature measurement of an atmospheric pressure plasma by millimeter wave interferometer. *Appl Phys Lett*. 2008;92(5):2007-2009. doi:10.1063/1.2840194

20. Hofmann S, Van Gessel AFH, Verreycken T, Bruggeman P. Power dissipation, gas temperatures and electron densities of cold atmospheric pressure helium and argon RF plasma jets. *Plasma Sources Sci Technol*. 2011;20(6). doi:10.1088/0963-0252/20/6/065010

21. Verreycken T, Van Gessel AFH, Pageau A, Bruggeman P. Validation of gas temperature measurements by OES in an atmospheric air glow discharge with water electrode using Rayleigh scattering. *Plasma Sources Sci Technol*. 2011;20(2). doi:10.1088/0963-0252/20/2/024002

22. Oshita T, Kawano H, Takamatsu T, Miyahara H, Okino A. Temperature Controllable Atmospheric Plasma Source. *IEEE Trans Plasma Sci*. 2015;43(6):1987-1992. doi:10.1109/TPS.2015.2428696

23. Kawano H, Takamatsu T, Matsumura Y, Miyahara H, Iwasawa A, Okino A. Influence of gas temperature in atmospheric non-equilibrium plasma on bactericidal effect. *Biocontrol Sci*. 2018;23(4):167-175. doi:10.4265/bio.23.167

24. Perekrestov R, Kudrna P, Tichý M. The deposition of titanium dioxide nanoparticles by means of a hollow cathode plasma jet in dc regime. *Plasma Sources Sci Technol*. 2015;24(3). doi:10.1088/0963-0252/24/3/035025

Accepted Manuscript

25. Zhang R, Luo G. The mode of gliding arc discharge and its characteristics. *Proc IEEE Int Conf Prop Appl Dielectr Mater*. 2018;2018-May:305-310. doi:10.1109/ICPADM.2018.8401270

26. Gerasimov A V., Kirpichnikov AP, Rachevsky LA. Determination of gas temperature in the plasmatron channel according to the known distribution of electronic temperature. *Therm Sci*. 2013;17(4):1251-1254. doi:10.2298/TSCI1304251G

27. Chen CJ, Li SZ. Spectroscopic measurement of plasma gas temperature of the atmospheric-pressure microwave induced nitrogen plasma torch. *Plasma Sources Sci Technol*. 2015;24(3). doi:10.1088/0963-0252/24/3/035017

28. Bruggeman P, Brandenburg R. Atmospheric pressure discharge filaments and microplasmas: Physics, chemistry and diagnostics. *J Phys D Appl Phys*. 2013;46(46). doi:10.1088/0022-3727/46/46/464001

29. Iseni S, Michaud R, Lefaucheux P, Sretenović GB, Schulz-Von Der Gathen V, Dussart R. On the validity of neutral gas temperature by emission spectroscopy in micro-discharges close to atmospheric pressure. *Plasma Sources Sci Technol*. 2019;28(6). doi:10.1088/1361-6595/ab1dfb

30. Knoerzer K, Murphy AB, Fresewinkel M, Sanguansri P, Coventry J. Evaluation of methods for determining food surface temperature in the presence of low-pressure cool plasma. *Innov Food Sci Emerg Technol*. 2012;15:23-30. doi:10.1016/j.ifset.2012.02.008

31. Mazouffre S, Echegut P, Dudeck M. A calibrated infrared imaging study on the steady state thermal behaviour of Hall effect thrusters. *Plasma Sources Sci Technol*. 2007;16(1):13-22. doi:10.1088/0963-0252/16/1/003

32. Fu W, Zhang C, Nie C, Li X, Yan Y. A high efficiency low-temperature microwave-driven atmospheric pressure plasma jet. *Appl Phys Lett*. 2019;114(25). doi:10.1063/1.5108538

33. Engelhard C, Scheffer A, Maue T, Hieftje GM, Buscher W. Application of infrared thermography for online monitoring of wall temperatures in inductively coupled plasma torches with conventional and low-flow gas consumption. *Spectrochim Acta - Part B At Spectrosc*. 2007;62(10):1161-1168. doi:10.1016/j.sab.2007.07.010

34. Dowling DP, Donegan M, Cullen PJ, Law VJ, Milosavljevic V. Importance of plasma thermal energy transfer for plasma jet systems. *IEEE Trans Plasma Sci*. 2014;42(10):2426-2427. doi:10.1109/TPS.2014.2326962

35. Jang J, Choe W, Peterson BJ, et al. Tomographic reconstruction of two-dimensional radiated power distribution during impurity injection in KSTAR plasmas using an infrared imaging video bolometer. *Curr Appl Phys*. 2018;18(4):461-468. doi:10.1016/j.cap.2018.01.009

36. Askari S, Levchenko I, Ostrikov K, Maguire P, Mariotti D. Crystalline Si nanoparticles below crystallization threshold: Effects of collisional heating in non-thermal atmospheric-pressure microplasmas. *Appl Phys Lett*. 2014;104(16). doi:10.1063/1.4872254

37. Bruggeman P, Iza F, Guns P, et al. Electronic quenching of OH(A) by water in atmospheric pressure plasmas and its influence on the gas temperature determination by OH(A-X) emission. *Plasma Sources Sci Technol*. 2010;19(1). doi:10.1088/0963-0252/19/1/015016

38. Motret O, Hibert C, Pellerin S, Pouvesle JM. Rotational temperature measurements in atmospheric pulsed dielectric barrier discharge - gas temperature and molecular fraction effects. *J Phys D Appl Phys*. 2000;33(12):1493-1498. doi:10.1088/0022-3727/33/12/311

39. Maguire P, Rutherford D, Macias-Montero M, et al. Continuous In-Flight Synthesis for On-Demand Delivery of Ligand-Free Colloidal Gold Nanoparticles. *Nano Lett*. 2017;17(3):1336-1343. doi:10.1021/acs.nanolett.6b03440

40. Bennet ED, Mahony CMO, Potts HE, et al. Precision charging of microparticles in plasma via the Rayleigh instability for evaporating charged liquid droplets. *J Aerosol Sci*. 2016;100:53-60.

Accepted Manuscript

doi:10.1016/j.jaerosci.2016.05.002

41. https://www.micro-epsilon.com/temperature-sensors/thermoMETER_CT_basic/?sLang=en.

42. Mariotti D. Nonequilibrium and effect of gas mixtures in an atmospheric microplasma. *Appl Phys Lett*. 2008;92(15):2006-2009. doi:10.1063/1.2912039

43. ABRAMZON B, SIRIGNANO W. Droplet vaporization model for spray combustion calculations. 1988;32(9):1605-1618. doi:10.2514/6.1988-636

44. Heinisch C, Wills JB, Reid JP, Tschudi T, Tropea C. Temperature measurement of single evaporating water droplets in a nitrogen flow using spontaneous raman scattering. *Phys Chem Chem Phys*. 2009;11(42):9720-9728. doi:10.1039/b908555f

Accepted Manuscript